A possible mechanism for confinement power degradation in the TJ-II stellarator

B. Ph. van Milligen, B. A. Carreras, C. Hidalgo, Á. Cappa, and TJ-II Team

Citation: Physics of Plasmas **25**, 062503 (2018); doi: 10.1063/1.5029881
View online: https://doi.org/10.1063/1.5029881
View Table of Contents: http://aip.scitation.org/toc/php/25/6
Published by the American Institute of Physics

A possible mechanism for confinement power degradation in the TJ-II stellarator

B. Ph. van Milligen,[1] B. A. Carreras,[2] C. Hidalgo,[1] Á. Cappa,[1] and TJ-II Team
[1]*CIEMAT - Laboratorio Nacional de Fusión, Avda. Complutense 40, 28040 Madrid, Spain*
[2]*Universidad Carlos III, Leganés, 28911 Madrid, Spain*

(Received 16 March 2018; accepted 18 May 2018; published online 7 June 2018)

This work uses the outward propagation of spontaneously generated fluctuations of the electron temperature to study heat transport in the TJ-II stellarator. Data from a set of experiments in which the heating power was scanned systematically are analyzed using the transfer entropy. The transfer entropy graph suggests there are at least two modes or channels of propagation: one channel is continuous, reminiscent of diffusion, while the other is non-local, activated mainly when the heating power is large. When the heating power is increased, the region of non-locality expands outwards, leading to the ubiquitously observed deterioration of confinement with heating power.
https://doi.org/10.1063/1.5029881

I. INTRODUCTION

Power degradation is a phenomenon, observed in all experimental devices based on the magnetic confinement of plasmas, that the energy confined in the plasma (W) increases less than linearly with the heating power. The observed scaling of the energy confinement time with heating power is $\tau_E \propto P^{\alpha_P}$, where $\alpha_P \simeq -0.6 \pm 0.1$.[1–5] Remarkably, this scaling holds across the board for the main types of magnetic fusion devices (tokamaks and stellarators) and hence must be due to a very basic mechanism, common to these devices.

Many mechanisms have been proposed to explain the phenomenon of power degradation. To name a few: plateau scaling,[4] enhanced microturbulence,[6] and Neoclassical tearing mode turbulence.[7]

One aspect of this conundrum is the observation of "profile stiffness," i.e., the fact that (electron) temperature profiles are relatively insensitive to changes in heating power deposition.[8,9] In line with the above, highly non-linear dependencies of transport coefficients on local plasma parameters were proposed to model this observation, typically denominated "critical gradient models."[10,11] Profile stiffness can be understood in the framework of plasma self-organization, according to which transport increases sharply when a threshold gradient is exceeded, similar to what happens in a paradigmatic sandpile.[12] The microscopic motivation for such models is based on the activation of micro-turbulence as gradients are increased.

However, careful analysis showed that even such complex local dependencies could not explain all observations,[1] and it was suggested that the transport coefficients should somehow depend directly on the input power, although it was not clarified by what mechanism.

The observation of the propagation of heat and cold pulses led to the suggestion that heat transport should be "non-local,"[13,14] meaning that the transport coefficients at one location somehow depend on the plasma parameters at another location. Of course, no causality-infringing "instantaneous influence" is suggested here, merely a communication that significantly exceeds diffusive speeds over distances much larger than microscopic plasma scales.

In summary, even after many years of intensive studies, this issue of what causes power degradation remains largely unsettled. Is transport local but non-linear (having nonlinear dependencies of the transport on local plasma parameters, such as "critical gradients")? Or is it non-local, and if so, what is the underlying mechanism[14]? Is there some mysterious direct dependency on the input power? Or is there some other ingredient that has not yet been considered? An important practical question is whether one can continue to model transport using diffusive models or should consider a paradigm shift towards fully non-local modelling.[15,16]

In this work, we propose exploring this issue experimentally by analyzing the radial propagation of small temperature perturbations. For this purpose, we study the scaling of transport with heating power, using a relatively new technique known as the transfer entropy, applied to Electron Cyclotron Emission (ECE) data in the TJ-II stellarator.

This paper is structured as follows: in Sec. II, the experimental setup and the analysis techniques are discussed. In Sec. III, we present the experimental results. In Sec. IV, we discuss the results and draw some conclusions.

II. EXPERIMENTAL SET-UP AND TECHNIQUES USED

The experiments reported here were performed in the 4-period TJ-II stellarator (magnetic field $B_T \simeq 1$ T, major radius $R_0 = 1.5$ m, and minor radius $\langle a \rangle \leq 0.22$ m). The magnetic configuration used is the "standard" magnetic configuration (labelled 100_44_64). The corresponding rotational transform profile ($\iota = \iota/2\pi$) as a function of normalized radius $|\rho| = |r|/a$ is shown in Fig. 1. Discharges were heated using Electron Cyclotron Resonant Heating (ECRH).

A. ECRH and ECE measurements

The ECRH system consists of two gyrotrons with a frequency of 53.2 GHz, allowing the injection of up to 2×300 kW of heating power (second harmonic, X-mode).[17] The heating power was varied in the range $200 \leq P_{ECRH} \leq 600$ kW, deposited centrally, in order to study the scaling

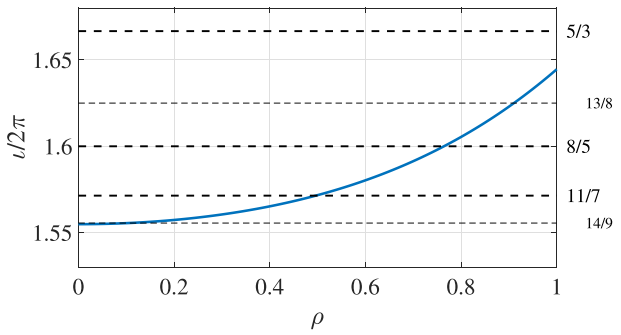

FIG. 1. ι profile for the standard magnetic configuration (100_44_64). Some rational values are indicated by horizontal dashed lines.

of confinement with heating power. The half width of the deposition profile is approximately $w_{\mathrm{ECRH}} \simeq 3$ cm.[18]

TJ-II disposes of a 12 channel Electron Cyclotron Emission (ECE) detection system to measure the local electron temperature T_e at up to 12 different radial positions along the midplane on the high magnetic field side of the plasma (at a toroidal angle of $\phi = 315°$), covering a significant part of the plasma minor radius (about 70%), with a radial resolution of about 1 cm.[19] The ECE channels are tuned to the second harmonic of the electron cyclotron frequency at various positions inside the plasma. The position of each channel is converted to a normalized radius, $\rho = r/a$, using the known (theoretical) magnetic configuration. By convention, positive ρ values correspond to the low field side of the plasma and negative ρ values correspond to the high field side. A few examples of T_e profiles measured by the ECE diagnostic, at various ECRH power levels, are shown in Fig. 2. Power degradation is almost visible to the naked eye: raising the power by a factor of 2.4, the electron temperature only goes up by a factor of 1.9.

B. Temperature fluctuations and propagation of perturbations

The ECRH power deposited in the core of the plasma causes spontaneous temperature fluctuations,[20,21] possibly related to the presence of rational surfaces in the core region

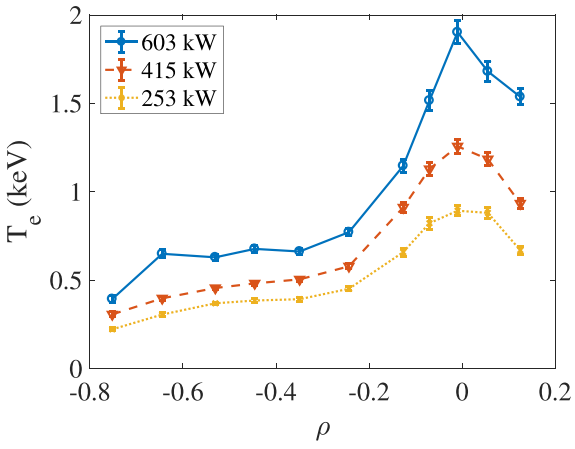

FIG. 2. Electron temperature profiles, measured by the ECE diagnostic, at various heating power levels.

of the plasma where the heat is deposited[22] and the concomitant generation of fast electrons.[23] These temperature fluctuations then lead to the outward propagation of small corresponding cascades or perturbations, similar to what has been reported in Ref. 24. We exploit this phenomenon to analyze heat transport outside the core power deposition region. For this purpose, we will use the transfer entropy technique described in Sec. II C below.

C. Transfer entropy

The transfer entropy is a technique from the field of Information Theory[25] that was recently applied for the first time in the context of fusion plasmas.[26] This nonlinear technique measures the "information transfer" between two signals, is directional, and uses all the information available in the two signals, regardless of amplitude or sign.

The transfer entropy is a measure of the causal relation or information flow between two time series. The transfer entropy between discretely sampled signals $y(t_i)$ and $x(t_i)$ quantifies the number of bits by which the prediction of the next sample of signal x can be improved by using the time history of not only the signal x itself, but also that of signal y.

In this work, we use a simplified version of the transfer entropy

$$T_{Y\to X} = \sum p(x_{n+1}, x_{n-k}, y_{n-k}) \log_2 \frac{p(x_{n+1}|x_{n-k}, y_{n-k})}{p(x_{n+1}|x_{n-k})}. \quad (1)$$

Here, $p(a|b)$ is the probability distribution of a conditional on b, $p(a|b) = p(a,b)/p(b)$. The probability distributions $p(a,b,c,\ldots)$ are constructed using m bins for each argument, i.e., the object $p(a,b,c,\ldots)$ has m^d bins, where d is the dimension (number of arguments) of p. The sum in Eq. (1) runs over the corresponding discrete bins. The number k can be converted to a "time lag" by multiplying it by the sampling rate. The construction of the probability distributions is done using "course graining," i.e., a low number of bins (here, $m = 3$), to obtain statistically significant results. For more information on the technique, please refer to Ref. 26. The value of the transfer entropy T, expressed in bits, can be compared with the total bit range, $\log_2 m$, equal to the maximum possible value of T, to help decide whether the transfer entropy is significant or not.

The statistical significance of the transfer entropy can be estimated by calculating T for two random (noise) signals.[27] Here, we will be analyzing time intervals with a typical duration of about 80 ms, corresponding to $N = 8 \times 10^3$ points, and the statistical significance level of T is of the order of 1×10^{-3}.

Regarding the interpretation of the transfer entropy, we note that it is a non-linear quantifier of information transfer and helps clarifying which fluctuating variables influence which others—without specifying the nature of this influence. In this sense, it is fundamentally different from the cross correlation, which is maximal for two identical signals ($x = y$), whereas the transfer entropy is exactly zero for two identical signals (as no information is gained by using the second, identical signal to help predicting the behavior of the first).

The transfer entropy has some remarkable properties. First, it is directional, a fact that provides a filter that preferentially selects information components related to (directional) propagation. Second, unlike linear tools such as the cross correlation or the conditional average, it does not depend on the temporal waveform or even the amplitude of the fluctuations, but merely on the time lag between x and y. This converts the technique in an exquisitely sensitive tool to study the propagation of perturbations in highly non-linear systems (such as fusion plasmas), in which perturbations tend to be deformed or change shape quickly as they propagate.

The value of the transfer entropy for the analysis of heat transport in a fusion device was clearly demonstrated in a recent paper.[28] There, the relation of the technique to the more common cross correlation was studied, concluding that the transfer entropy supersedes the cross correlation when analyzing the propagation of perturbations in a turbulent environment. Furthermore, it was observed that the time lag of the transfer entropy maximum is closely related to the phase delay obtained from the Fourier analysis of modulation experiments. Hence, the transfer entropy delivers information highly relevant to plasma transport.

III. EXPERIMENTS

The series of experiments reported here were performed on April 16, 2008. The data correspond to a set of 19 discharges at 9 different levels of P_{ECRH}. The plasma parameters (other than T_e) were kept as constant as possible throughout this set of discharges. The electron temperature (cf. Fig. 2) and density profiles are similar to those shown in Ref. 18. The ion temperature gradients are small.[29] Figure 3 shows the variation of line averaged electron density, $\langle n_e \rangle$ from interferometry, and plasma energy content, W, obtained from a diamagnetic loop. It is seen that the line averaged electron density is fairly constant, while the variation of the plasma energy content is consistent with the expected scaling for magnetically confined plasmas: $W \propto P_{\mathrm{ECRH}}^{0.4}$, implying $\tau_E = W/(P - dW/dt) \simeq W/P \propto P_{\mathrm{ECRH}}^{-0.6}$.

A. The radial propagation of perturbations

The radial propagation of electron temperature perturbations in TJ-II has been studied in a previous work.[30] Figure 4 shows two examples from the current series of discharges, at low and high ECRH power. The transfer entropy, $T_{X\to Y}(\tau)$, is calculated between a reference channel X (here, the ECE channel located at $\rho_{\mathrm{ref}} \simeq -0.07$) and the other ECE channels, Y, whose location is indicated by white circles in the figure. The TE is calculated using 80 ms of data in the steady state; the sampling rate of the ECE channels is 100 kHz. As noted above, the TE yields zero for the case $T_{X\to X}$ (between the reference channel and itself). For small values of $|\rho|$, in the ECRH power deposition zone, the TE is large at very small values of the time lag τ. However, for positions away from this zone, the TE peaks at a time lag that is significantly larger than zero, corresponding to the propagation of perturbations and ruling out instrumental effects due to, e.g., small optical depth, which would lead to peaking at time lags equal to zero.

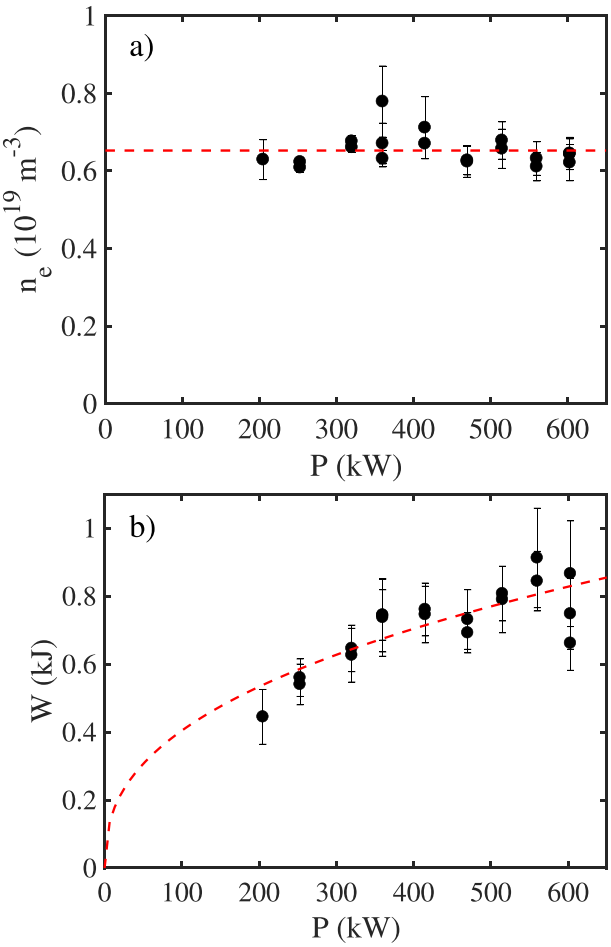

FIG. 3. (a) Line averaged density (from interferometry) versus P_{ECRH}. (b) Plasma energy content versus P_{ECRH}.

The pattern of propagation one observes is always very similar, as reported in an earlier work.[30] Propagation is relatively fast in some regions, but appears to stagnate at specific positions (e.g., $\rho \simeq -0.35$ and -0.55 in the figure). The stagnation zones appear to be associated with major rational surfaces. In the cited work, it was suggested that at these locations, resonant fluctuations tend to create shear flow layers, leading to minor transport barriers, explaining why transport tends to slow down there. The zones of rapid propagation may involve non-local effects associated with mode coupling, leading to "jumping" behavior.

Comparing the low and high power cases shown in the figure, one observes a relatively smooth "plume" of propagating perturbations in the low power case, propagating outward from $\rho = \rho_{\mathrm{ref}}$. The main body of the plume occurs in the range $-0.35 < \rho < -0.07$, although a rather weak continuation of the plume reaches about $\rho \simeq -0.55$, where some stagnation may be visible. This situation would be roughly consistent with "normal" diffusive propagation. However, in the high power case, the plume clearly stagnates at $\rho \simeq -0.35$, developing a long horizontal "tail"; yet for $\tau \simeq 0.2$ ms, a second propagation branch appears at $\rho \simeq -0.55$, with an amplitude comparable to or greater than the first branch. Note that this

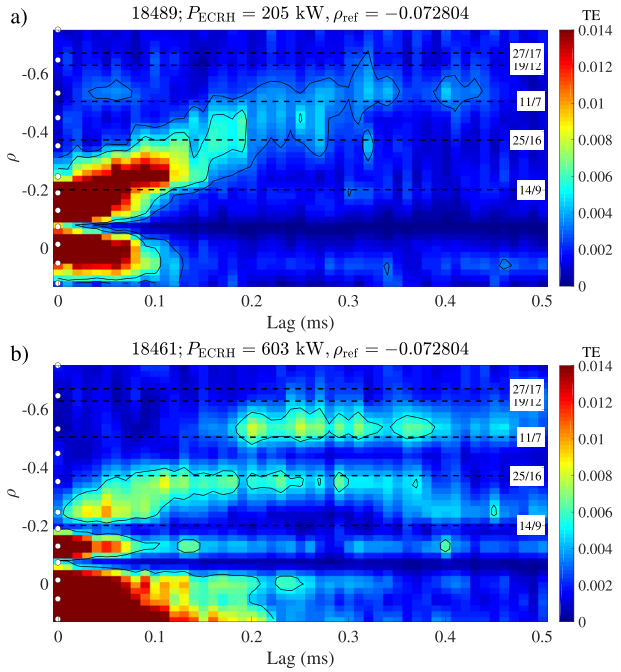

FIG. 4. Examples of transfer entropy calculated from ECE data, using $\rho_{ref} \simeq -0.07$, at (a) $P_{ECRH} = 205$ kW and (b) $P_{ECRH} = 603$ kW. The color scale indicates the value of T. The ECE channel positions are indicated with white circles. The approximate location of some major rational surfaces is indicated by horizontal dashed lines; the line labels specify the corresponding rotational transform, n/m.

response occurs without any detectable response at $\rho \simeq -0.45$, so that the perturbations seem to have "jumped over" this intermediate position. The perturbations at $\rho \simeq -0.55$ have a stronger causal link to ρ_{ref} (higher value of TE) than in the low power case. The stronger causal response at $\rho \simeq -0.55$ may be related to power degradation, as perturbations seem to be better able to reach this position and influence turbulence there, possibly implying a more intense radial transport from ρ_{ref} to $\rho \simeq -0.55$ in the high power case. We will attempt to quantify this idea in Sec. III B.

B. Effective diffusivities

The transfer entropy, discussed above, quantifies the propagation of "information," rather than heat. Therefore, it is not immediately obvious how the reported findings relate to the electron heat transport coefficient, χ_e, used in traditional transport models for magnetically confined plasmas. On the other hand, diffusion is, in some sense, a "geometric" process (the spreading in space of an initially concentrated perturbation), as reflected in the dimensionality of the diffusion coefficient, χ_e (m^2/s), which involves a length and a time, but no temperature or energy. Thus, it is possible that the "spreading of information" measured by the TE is related to the "spreading of heat" measured by χ_e. From another point of view, the transport of information is mediated by the transport of (fluctuations of) heat, which is what is measured by the ECE diagnostic, hence the transport of information should be equivalent to the transport of heat in this case, or at least cannot exceed it (since the information cannot go where the heat, which "carries" it, does not go).

To shed some light on this issue, we define an effective diffusivity, χ_{eff}, and observe how it behaves. For this purpose, we first quantify the time evolution of the centre of gravity of the propagating perturbations by calculating the mean radius of the propagating information as follows:

$$\langle \rho \rangle = \frac{\int T_{\rho_{ref} \to \rho} \rho d\rho}{\int T_{\rho_{ref} \to \rho} d\rho}, \tag{2}$$

i.e., the weighted mean of the radius, using the TE $T_{\rho_{ref} \to \rho}$ between the reference position and position ρ as the weight. The integration only includes negative values of ρ (the low field side of the plasma). This quantity is evaluated for each value of the lag τ.

Figure 5 shows two examples of $\langle r \rangle = -\langle \rho \rangle a$ as a function of $\sqrt{\tau}$ based on TE graphs such as those shown in Fig. 4; although here, we used the ECE channel at $\rho \simeq -0.35$ as reference in order to obtain an estimate of χ_{eff} for $|\rho| > 0.5$ ($\langle r \rangle > 0.1$). A straight section of this curve allows fitting a straight line and making an estimate of the effective diffusivity (equal to the square of the slope of this line), namely, $\chi_{eff} \simeq 1 - 4$ m^2/s. Note that this value is comparable to the global electron heat diffusivity determined in earlier work, using modulation experiments,[18] namely, $\chi_e \simeq 2$ m^2/s, thus confirming the close relation between the effective (TE) and electron heat diffusivities.[28]

C. Effective local diffusivities as a function of radius and P_{ECRH}

In this section, we estimate local values of the effective diffusivity, χ_{eff}, for all available discharges and using different ECE channels as a reference. This allows us to make estimates of χ_{eff} at different radial positions.

The result for the three lowest values of P_{ECRH} is shown in Fig. 6. The three cases show a similar radial dependence. The values of the effective diffusivity are high in the inner part of the plasma and drop as one moves outward (recall that the plasma minor radius is $a = 0.2$ m). We note that this is similar to what was observed in previous work, using traditional techniques (Figs. 13 and 14 in Ref. 18).

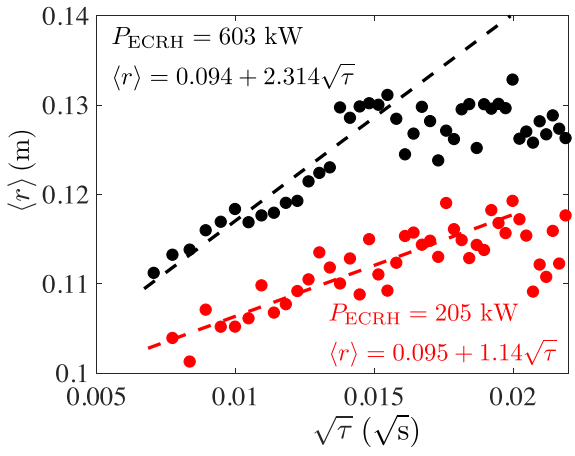

FIG. 5. Mean radius of propagation, $\langle r \rangle$, versus the square root of the time lag, τ.

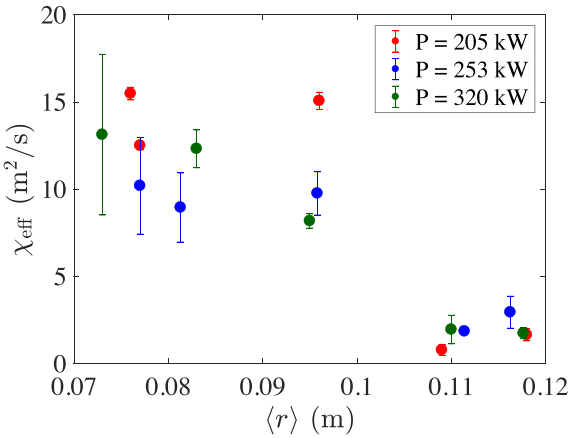

FIG. 6. Radial dependence of the effective diffusivity for three values of $P_{\rm ECRH}$ in the low power range.

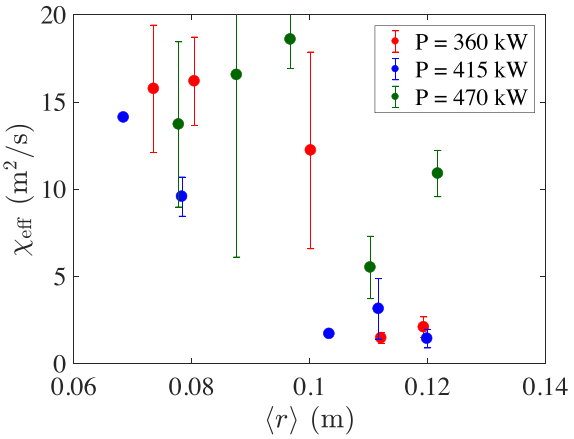

FIG. 8. Radial dependence of the effective diffusivity for three values of $P_{\rm ECRH}$ in the medium power range.

Figure 7 shows a similar result for the three highest values of $P_{\rm ECRH}$. There is a clear change from Fig. 6. In the inner region, the effective diffusivity has decreased, while it has increased in the outer region. Thus, in this power range, the radial dependence of the effective diffusivity is weaker.

For simplicity, we assume that the effective diffusivity is a combination of standard diffusive transport plus a variable non-local component (cf. Sec. III A). Since ECRH power is mostly deposited in the core, the effect of the heating is to first facilitate the non-local transport in the inner part of the plasma. As the heating increases, this non-local effect expands to regions located further outward. The plasma volume increases as r^2, so even a relatively small increase in transport in the outer region will have a significant effect on global confinement.

In Fig. 8, we plotted an equivalent graph to Figs. 6 and 7 for intermediate values of $P_{\rm ECRH}$. One observes that the transition from low to higher power behavior possibly occurs in the range of 400 kW–500 kW.

IV. DISCUSSION AND CONCLUSIONS

The analysis of the discharges from an ECRH power scan in TJ-II suggests a mechanism to explain the deterioration of confinement with heating power. It appears that radial heat transport is not a smooth and continuous process, but involves "stagnation zones" or "mini-transport barriers"[28] (reminiscent of an "$E \times B$" staircase,[31] likely associated with localized zones with the enhanced sheared flow) where transport tends to slow down. On the other hand, transport may also experience rapid radial (non-local) "jumps," connecting apparently separate regions across the "mini-transport barriers".

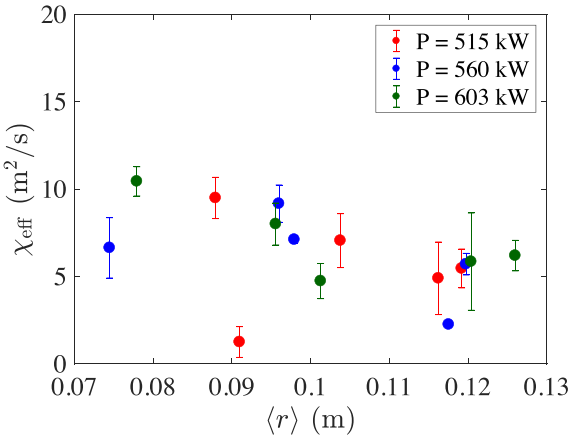

FIG. 7. Radial dependence of the effective diffusivity for three values of $P_{\rm ECRH}$ in the high power range.

The combination of these two ingredients and the findings of Sec. III C allow us to suggest a possible mechanism to explain the degradation of confinement with increasing heating power. When the ECRH power is increased but still low, non-local transport in the inner part of the plasma is enhanced first—detected here as a high value of the effective diffusivity. As the heating increases further, this non-local effect expands towards more outlying regions of the plasma while the effective diffusivity in the core region drops. This increased importance of non-local transport in zones that are located further outward would lead to the deterioration of confinement.

Considering the hypothetical explanations of power degradation cited in the introduction, we observe that the rapid transport channel is consistent with the "non-local" hypothesis, while its activation with increased heating power is consistent with the "critical gradient" hypothesis.

The question remains, however, to what underlying physical mechanism this "non-local" transport component corresponds. In earlier studies,[28,30] we suggested that this mechanism involves the radial coupling of MHD turbulence, so that the fast "non-local" transport channel is based on the transmission of turbulent energy via the magnetic field. We note that such a mechanism would imply an important role for rational magnetic surfaces in turbulent transport, as indeed evidenced by some previous studies.[32,33]

ACKNOWLEDGMENTS

The authors would like to thank the TJ-II Team for its continued support. This research is sponsored in part by the Ministerio de Economía y Competitividad of Spain under Project No. ENE2015-68206-P. This work has been carried

out within the framework of the EUROfusion Consortium and has received funding from the Euratom research and training programme 2014–2018 under Grant Agreement No. 633053. The views and opinions expressed herein do not necessarily reflect those of the European Commission.

[1]U. Stroth, L. Giannone, H. J. Hartfuss *et al.*, "Fast transport changes and power degradation in the W7-AS stellarator," Plasma Phys. Controlled Fusion **38**, 611 (1996).
[2]B. A. Carreras, "Progress in anomalous transport research in toroidal magnetic confinement systems," IEEE Trans. Plasma Sci. **25**(6), 1281 (1997).
[3]E. J. Doyle, W. A. Houlberg, Y. Kamada *et al.*, "Chapter 2: Plasma confinement and transport," Nucl. Fusion **47**(6), S18 (2007).
[4]A. Dinklage, H. Maaßberg, R. Preuss *et al.*, "Physical model assessment of the energy confinement time scaling in stellarators," Nucl. Fusion **47**(9), 1265 (2007).
[5]M. Hirsch, J. Baldzuhn, C. Beidler *et al.*, "Major results from the stellarator Wendelstein 7-AS," Plasma Phys. Controlled Fusion **50**, 053001 (2008).
[6]D. L. Brower, C. X. Yu, R. V. Bravenec *et al.*, "Confinement degradation and enhanced microturbulence as long-time precursors to high-density-limit tokamak disruptions," Phys. Rev. Lett. **67**(2), 200 (1991).
[7]L. Bardóczi, T. A. Carter, R. J. La Haye *et al.*, "Impact of neoclassical tearing mode–turbulence multi-scale interaction in global confinement degradation and magnetic island stability," Phys. Plasmas **24**, 122503 (2017).
[8]F. Wagner, O. Gruber, K. Lackner *et al.*, "Experimental study of the principles governing tokamak transport," Phys. Rev. Lett. **56**(20), 2187 (1986).
[9]Yu. N. Dnestrovskij, K. A. Razumova, A. J. H. Donné *et al.*, "Self-consistency of pressure profiles in tokamaks," Nucl. Fusion **46**, 953 (2006).
[10]F. Ryter, C. Angioni, M. Beurskens *et al.*, "Experimental studies of electron transport," Plasma Phys. Controlled Fusion **43**, A323 (2001).
[11]X. Garbet, P. Mantica, F. Ryter *et al.*, "Profile stiffness and global confinement," Plasma Phys. Controlled Fusion **46**, 1351 (2004).
[12]B. A. Carreras, V. E. Lynch, P. H. Diamond *et al.*, "On the stiffness of the sand pile profile," Phys. Plasmas **5**(4), 1206 (1998).
[13]K. W. Gentle, R. V. Bravenec, G. Cima *et al.*, "An experimental counterexample to the local transport paradigm," Phys. Plasmas **2**(6), 2292 (1995).
[14]K. Ida, Z. Shi, H. J. Sun *et al.*, "Towards an emerging understanding of non-locality phenomena and non-local transport," Nucl. Fusion **55**(1), 013022 (2015).
[15]B. Ph. van Milligen, R. Sánchez, and B. A. Carreras, "Probabilistic finite-size transport models for fusion: Anomalous transport and scaling laws," Phys. Plasmas **11**(5), 2272 (2004).
[16]B. Ph. van Milligen, B. A. Carreras, and R. Sánchez, "Uphill transport and the probabilistic transport model," Phys. Plasmas **11**(8), 3787 (2004).
[17]A. Fernández, J. M. de la Fuente, D. Ganuza *et al.*, "Performance of the TJ-II ECRH system with the new 80 kV 50 A high voltage power supply," Fusion Eng. Des. **84**(2-6), 772 (2009).
[18]S. Eguilior, F. Castejón, E. de la Luna *et al.*, "Heat wave experiments on TJ-II flexible heliac," Plasma Phys. Controlled Fusion **45**, 105 (2003).
[19]E. de la Luna, J. Sánchez, V. Tribaldos *et al.*, "Multichannel electron cyclotron emission radiometry in TJ-II stellarator," Rev. Sci. Instrum. **72**(1), 379 (2001).
[20]T. Happel, A. Bañón Navarro, G. D. Conway *et al.*, "Core turbulence behavior moving from ion-temperature-gradient regime towards trapped-electron-mode regime in the ASDEX Upgrade tokamak and comparison with gyrokinetic simulation," Phys. Plasmas **22**(3), 032503 (2015).
[21]C. Hidalgo, A. Chmyga, L. Eliseev *et al.*, "On the influence of ECRH on neoclassical and anomalous mechanisms using a dual heavy ion beam probe diagnostic in the TJ-II stellarator," in *26th IAEA Fusion Energy Conference Proceedings* (2016), p. EX–P7/44.
[22]T. Estrada, E. de la Luna, E. Ascasíbar *et al.*, "Transient behaviour in the plasma core of TJ-II stellarator and its relation with rational surfaces," Plasma Phys. Controlled Fusion **44**, 1615 (2002).
[23]L. García, M. A. Ochando, B. A. Carreras *et al.*, "Effect of fast electrons on the stability of resistive interchange modes in the TJ-II stellarator," Phys. Plasmas **23**, 062319 (2016).
[24]P. A. Politzer, "Observation of avalanchelike phenomena in a magnetically confined plasma," Phys. Rev. Lett. **84**(6), 1192 (2000).
[25]T. Schreiber, "Measuring information transfer," Phys. Rev. Lett. **85**(2), 461 (2000).
[26]B. Ph. van Milligen, G. Birkenmeier, M. Ramisch *et al.*, "Causality detection and turbulence in fusion plasmas," Nucl. Fusion **54**, 023011 (2014).
[27]B. Ph. van Milligen, B. A. Carreras, L. García *et al.*, "The causal relation between turbulent particle flux and density gradient," Phys. Plasmas **23**, 072307 (2016).
[28]B. Ph. van Milligen, U. Hoefel, J. H. Nicolau *et al.*, "Study of radial heat transport in W7-X using the transfer entropy," Nucl. Fusion **58**, 076002 (2018).
[29]J. M. Fontdecaba, F. Castejón, R. Balbín *et al.*, "Energy-resolved neutral particle fluxes in TJ-II ECRH plasmas," Fusion Sci. Technol. **46**, 271 (2004).
[30]B. Ph. van Milligen, J. H. Nicolau, L. García *et al.*, "The impact of rational surfaces on radial heat transport in TJ-II," Nucl. Fusion **57**(5), 056028 (2017).
[31]G. Dif-Pradalier, G. Hornung, Ph. Ghendrih *et al.*, "Finding the elusive E × B staircase in magnetized plasmas," Phys. Rev. Lett. **114**, 085004 (2015).
[32]N. J. Lopes Cardozo, G. M. D. Hogeweij, M. de Baar *et al.*, "Electron thermal transport in RTP: Filaments, barriers and bifurcations," Plasma Phys. Controlled Fusion **39**, B303 (1997).
[33]S. J. Wukitch, R. L. Boivin, P. T. Bonoli *et al.*, "Double transport barrier experiments on Alcator C-Mod," Phys. Plasmas **9**, 2149 (2002).